Turbofan Engine Sizing and Tradeoff Analysis via Signomial Programming

Martin A. York[1], Warren W. Hoburg[2], and Mark Drela[3]
Massachusetts Institute of Technology, Cambridge, MA, 02139

This paper presents a full 1D core+fan flowpath turbofan optimization model, based on first principles, and meant to be used during aircraft conceptual design optimization. The model is formulated as a signomial program, which is a type of optimization problem that can be solved locally using sequential convex optimization. Signomial programs can be solved reliably and efficiently, and are straightforward to integrate with other optimization models in an all-at-once manner. To demonstrate this, the turbofan model is integrated with a simple commercial aircraft sizing model. The turbofan model is validated against the Transport Aircraft System OPTimization turbofan model as well as two NASA Numerical Propulsion Simulation System turbofan models. Four integrated engine/aircraft parametric studies are performed, including a 2,460 variable multi-mission optimization that solves in 28 seconds.

Nomenclature

a_i = speed of sound at station i
α = engine by-pass ratio
α_{OD} = nominal on design by-pass ratio
α_{+1} = one plus engine by-pass ratio
A_i = station flow area
c_k = constant in a monomial, posynomial, or signomial
C_{D_0} = aircraft profile drag coefficient
C_L = aircraft lift coefficient
C_{p_i} = working fluid constant pressure specific heat at station i
D = drag force
η_{HP} = high pressure shaft power transmission efficiency
η_{LP} = low pressure shaft power transmission efficiency
η_{B} = combustor efficiency
F = total engine thrust
f_c = cooling flow by-pass ratio ($\dot{m}_{\text{cool}}/\dot{m}_{\text{core}}$)
f_{f} = fuel/air ratio
f_o = one minus the percent of core mass flow bled for pressurization, electrical generation, etc.
$f_{\text{f+1}}$ = one plus the fuel/air ratio
F_6 = core engine thrust
F_8 = fan engine thrust
F_{sp} = overall specific thrust
γ_i = ratio of working fluid specific heats at station i
G_{f} = fan gearing ratio
h_{t_i} = stagnation enthalpy at station i
h_i = static enthalpy at station i
I_{sp} = specific impulse

---

[1] Graduate Student, Department of Aeronautics and Astronautics.
[2] Assistant Professor, Department of Aeronautics and Astronautics.
[3] Terry J. Kohler Professor, Department of Aeronautics and Astronautics.

L = temperature lapse rate in the troposphere
N_{f} = normalized fan spool speed
N_1 = normalized LPC spool speed
N_2 = normalized HPC spool speed
K = induced drag correction factor
$\dot{m}_{\mathrm{core}}$ = core engine mass flow
$\dot{m}_{\mathrm{core_D}}$ = nominal on design core engine mass flow
$\dot{m}_{\mathrm{fan}}$ = fan mass flow
$\bar{m}_i$ = corrected mass flow at station i
$\dot{m}_{\mathrm{total}}$ = total engine mass flow
M_i = Mach number at engine station i
$m(u)$ = monomial function of u
P = atmospheric pressure
P_i = static pressure at station i
π_{b} = combustor pressure ratio
π_{D} = diffuser pressure ratio
π_{f} = fan pressure ratio
$\pi_{\mathrm{f_D}}$ = fan on design pressure ratio
π_{fn} = fan nozzle pressure ratio
π_{HPC} = high pressure compressor pressure ratio
$\pi_{\mathrm{HPC_D}}$ = high pressure compressor on design pressure ratio
π_{LPC} = low pressure compressor pressure ratio
$\pi_{\mathrm{LPC_D}}$ = low pressure compressor on design pressure ratio
P_{SL} = sea level pressure
P_{t_0} = stagnation pressure at engine station i
$p(u)$ = posynomial function of u
R = specific gas constant
ρ = air density
r_{uc} = cooling flow velocity ratio
S = aircraft wing area
$s(u)$ = signomial function of u
T = atmospheric temperature
T_i = static temperature at engine station i
T_{SL} = sea level temperature
TSFC= thrust specific fuel consumption
T_{t_i} = stagnation temperature at engine station i
u = vector of all decision variables
u_c = cooling flow velocity
u_i = flow velocity at station i
V = aircraft velocity
W_{engine} = engine weight
Z_i = total/static temperature ratio

Acronyms

BPR = by pass ratio
FPR = fan pressure ratio
GP = geometric program
HP = high pressure
HPC = high pressure compressor
HPT = high pressure turbine
LP = low pressure
LPC = low pressure compressor
LPT = low pressure turbine
NLP = nonlinear program

NPSS = Numerical Propulsion Simulation System
OPR = overall pressure ratio
SP = signomial program
TASOPT = Transport Aircraft System OPTimization
TOC = top of climb

I. Introduction

A key goal of conceptual aircraft design is to quantify basic trade offs between competing mission requirements and between the various aircraft sub-systems. For an exhaustive study, multiple design parameter sweeps must be performed, ideally with an optimum conceptual aircraft produced for each point examined. Because typical aircraft design-parameter spaces are quite large, such trade studies demand a reliable and efficient system-level optimization method. The majority of current multidisciplinary design optimization (MDO) tools rely on systems of black boxes and take hours to days to arrive at a single solution. This makes it difficult to explore the system-level Pareto frontier[1]. To greatly improve the speed and effectiveness of the aircraft conceptual design process, Hoburg et al.[2] and Kirschen et al.[3] have proposed formulating aircraft conceptual design models as geometric programs (GP) or signomial programs (SP), which can enable optimization problems with thousands of design variables to be reliably solved on laptop computers in a matter of seconds.

Such speed and reliability is possible because these formulations can be solved via convex optimization (in the case of GP), or via sequential convex optimization (in the case of SP). One limitation of GP methods is that all physical model equations must be posed as either posynomial inequality constraints or monomial equality constraints, which at first seems far too restrictive. One objective of this paper is to show that this is not necessarily the case, and that even quite complex physical models can be recast into the necessary forms. This is accomplished in two ways. First, many, but not all, expressions that arise in turbofan design are directly compatible with GP or can be closely approximated by posynomial constraints. Second, relationships that are not directly GP-compatible are often SP-compatible. SP is a non-convex extension of GP that can be solved locally as a sequence of GPs. While SPs sacrifice guarantees of global optimality, they can be solved far more reliably than general nonlinear programs (NLPs).

The specific example considered is the turbofan model in the Transport Aircraft System OPTimization (TASOPT)[4] conceptual design tool, which uses traditional optimization techniques. This model is a full 1D core+fan flowpath simulation based on first principles, which here will be recast into an SP-compatible form. This enables the construction of SP-compatible aircraft conceptual design models that address the complex design tradeoffs between engine and airframe parameters by treating the parameters as design variables. Such methods can produce much more realistic and higher-fidelity conceptual designs as starting points for subsequent preliminary and detailed design, with more reliability and much less time than would be required by the alternative MDO methods that combine traditional engine and airframe modules.

The SP-compatible engine model developed here is compared against TASOPT and two NASA Numerical Propulsion Simulation System (NPSS)[5] models to demonstrate that it produces the correct results. To demonstrate its effectiveness for SP aircraft optimization, the model is integrated into a simple commercial transport aircraft sizing optimization problem. Example aircraft parametric studies are presented, including a 2,460 variable multi-mission optimization problem that solves in 28 seconds.

II. Optimization Formulation

A. Model Architecture

The presented engine model is formulated as a single multi-point optimization problem with no engine on/off design point distinctions. All constraints are applied at every point in the flight, and the model selects the engine which most optimally meets all constraints. This, coupled with the fact SPs are solved all at once (i.e. there is no order of operations), greatly simplifies integrating the engine into a full aircraft system model. Figure 1 illustrates the engine model's overall architecture.

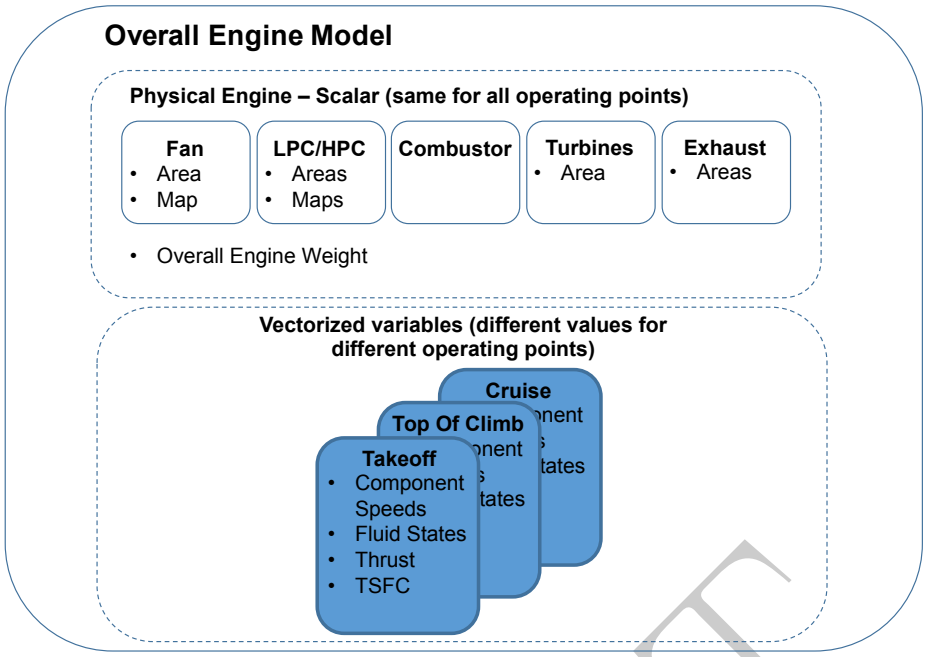

Fig. 1 Engine model architecture.

B. Solution Method

The models in this paper consist of sets of constraints that are compatible with SP. All SPs presented in this paper were solved on a laptop computer using a combination of GPkit[6] and MOSEK[7]. GPkit, developed at MIT, is a python package that enables the fast and intuitive formulation of geometric (GP) and signomial programs. GPkit has a built in heuristic for solving SPs as a series of GP approximations. GPkit binds with open source and commercial interior point solvers to solve individual GPs. For the purposes of this paper, the interior point solver MOSEK was used with an academic license.

C. Geometric Programming

Introduced in 1967 by Duffin et al. [8], a geometric program (GP) is a type of constrained optimization problem that becomes convex after a logarithmic change of variables. Modern interior point methods allow a typical sparse GP with tens of thousands of decision variables and tens of thousands of constraints to be solved in minutes on a desktop computer [9]. These solvers do not require an initial guess and guarantee convergence to a *global* optimum, assuming a feasible solution exists. If a feasible solution does not exist, the solver will return a certificate of infeasibility. These impressive properties are possible because a GP's objective and constraints consist of only monomial and posynomial functions, which can be transformed into convex functions in log space.

A monomial is a function of the form

$$m(\mathbf{u}) = c\prod_{j=1}^{n} u_j^{a_j} \tag{1}$$

where $a_j \in \mathbb{R}, c \in \mathbb{R}_{++}$ and $u_j \in \mathbb{R}_{++}$. An example of a monomial is the common expression for lift, $\frac{1}{2}\rho V^2 C_L S$. In this case, $\mathbf{u} = (\rho, V, C_L, S)$, $c = 1/2$, and $a = (1, 2, 1, 1)$.

A posynomial is a function of the form

$$p(\mathbf{u}) = \sum_{k=1}^{K} c_k \prod_{j=1}^{n} u_j^{a_{jk}} \tag{2}$$

where $a_{jk} \in \mathbb{R}, c_k \in \mathbb{R}_{++}$ and $u_j \in \mathbb{R}_{++}$. A posynomial is a sum of monomials. Therefore, all monomials are also one-term posynomials.

A GP minimizes a posynomial objective function subject to monomial equality and posynomial inequality constraints. A GP written in standard form is

$$\begin{aligned} &\text{minimize } p_0(\mathbf{u}) \\ &\text{subject to } p_i(\mathbf{u}) \leq 1, i = 1, ..., n_p, \\ &m_i(\mathbf{u}) = 1, i = 1, ..., n_m \end{aligned} \tag{3}$$

where p_i are posynomial functions, m_i are monomial functions, and $\mathbf{u} \in \mathbb{R}^n_{++}$ are the decision variables. Once a problem has been formulated in the standard form (Equation 3), it can be solved efficiently.

D. Signomial Programming

It is not always possible to formulate a design problem as a GP. This motivates the introduction of signomials. Signomials have the same form as posynomials

$$s(\mathbf{u}) = \sum_{k=1}^{K} c_k \prod_{j=1}^{n} u_j^{a_{jk}} \tag{4}$$

but the coefficients, $c_k \in \mathbb{R}$, can now be any (including non-positive) real numbers.

A signomial program (SP) is a generalization of GP where the inequality constraints can be composed of signomial constraints of the form $s(u) \leq 0$.. The log transform of an SP is not a convex optimization problem, but is a difference of convex optimization problem that can be written in log-space as

$$\begin{aligned} &\text{minimize } f_0(\mathbf{x}) \\ &\text{subject to } f_i(\mathbf{x}) - g_i(\mathbf{x}) \leq 0, i = 1, ..., m \end{aligned} \tag{5}$$

where f_i and g_i are convex.

There are multiple algorithms that reliably solve signomial programs to *local* optima [10, 11]. This is done by solving a sequence of GPs, where each GP is a local approximation to the SP, until convergence occurs. It is worth noting that the introduction of even a single signomial constraint to any GP turns the GP into a SP, thus losing the guarantee of solution convergence to a global optimum. Despite the possibility of convergence to a local, not global, optimum, SPs are a powerful tool. The convex approximation, $\hat{f}(x)$, to the non-convex signomial in log-space, $f(x) - g(x)$, is constructed such that it always satisfies

$$\hat{f}(x) \geq f(x) - g(x) \quad \forall \quad x \tag{6}$$

In other words, for each constraint, the feasible set of the convex approximation $\hat{f}(x) \leq 0$ is a subset of the original SP's feasible set, $f(x) - g(x) \leq 0$. This means SP inequalities do not require a trust region, removing the need for trust region parameter tuning and making solving SPs substantially more reliable than solving general nonlinear programs. Figure 2, where a series of convex (GP compatible) constraints approximates a non-convex parabolic drag polar in log space, illustrates this property.

E. Signomial Equality Constraints

The previously presented difference of convex technique works only for signomial inequality, posynomial inequality, and monomial equality or inequality constraints. Signomial equality constraints can be approximated by monomials as shown in Figure II E and may require a trust region. Trust regions were not used in the presented model. Signomial equalities are the least desirable type of constraint due the approximations involved. Most constraints in this work were relaxed to inequalities and checked for tightness by GPkit[6], but five signomial equalities are used. For additional details on how signomial equalities are approximated, see Opgenoord et al.[12]. For intuition on when signomial equality constraints are required, see Appendix B.

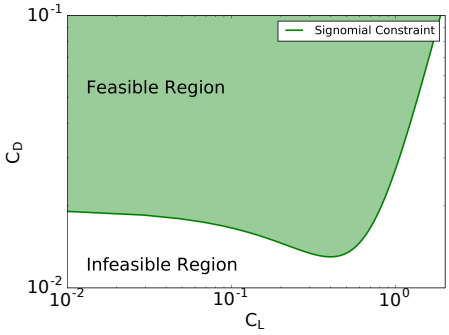

(a) Signomial inequaltiy drag constraint

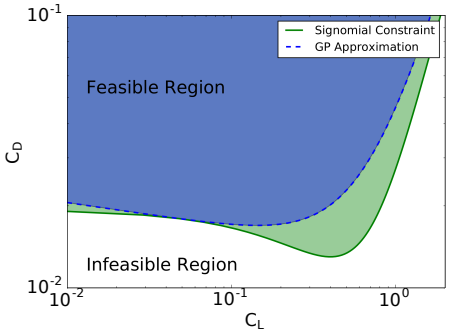

(b) Convex approximation about $C_L = 0.05$.

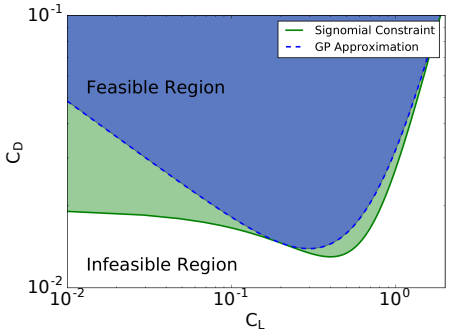

(c) Convex approximation about $C_L = 0.20$.

Fig. 2 A signomial inequality constraint and GP approximations about two different points.

III. Terminology

Before proceeding, it is useful to introduce some of the vocabulary used to describe this work.

A. Models

A model is a set of GP and/or SP compatible constraints. The input to a model is the value of any fixed variables or constants appearing the model. Two models that share variables may be linked by concatenating their constraints.

B. GP- and SP-compatibility

A constraint is GP-compatible if it can be written as either a monomial equality (equation 1) or a posynomial inequality (equation 2). A model is GP-compatible if its objective is a monomial or posynomial and all its constraints are GP compatible. A constraint is SP-compatible if it can be written as a signomial inequality (equation 4) or equality. A model is SP-compatible if its objective is a monomial, posynomial, or ratio of posynomials and all its constraints can be written as either monomial equalities, posynomial inequalities, signomial inequalities, or signomial equalities.

C. Static and Performance Models

The presented model is a multi-point optimization problem. To formulate the multi-point problem, two models are created for each engine component - a static and a performance model. The static model contains all variables and constraints that do not change between operating points, such as engine weight and nozzle areas. Performance models contain all constraints and variables that do change between operating points. For example, all constraints involving fluid states are contained in performance models. To simulate multiple engine operating points, the performance models are vectorized. When a model is vectorized, all the variables it contains become vectors,

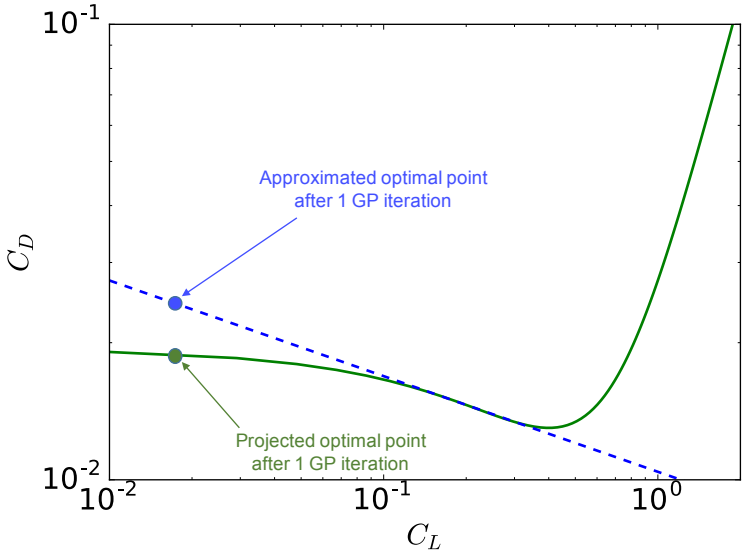

Fig. 3 The signomial equality constraint $C_D = f(C_L)$ and its approximation.

with each element corresponding to a different engine operating point. Figure 1 provides a visual representation of static and performance models.

IV. Model Derivation

Constraint derivation follows the general framework of the TASOPT turbofan model[4], with minor changes to facilitate the removal on the on-design/off-design distinction. TASOPT station numbering was adopted and is presented in Figure 4. The model assumes a two spool engine with two compressors and two turbines. The model can support a geared fan. Values of C_p and γ are assumed for each engine component and presented in Table 1. The following sections present assumptions, modeling techniques, and the model's constraints.

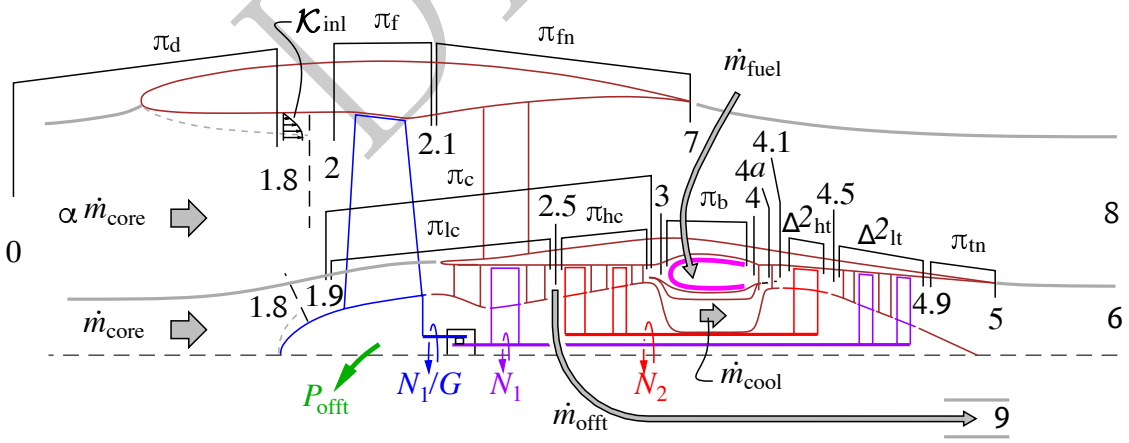

Fig. 4 TASOPT engine station numbering, which was adopted for this paper.

Table 1 Assumed gas properties for each engine component

Engine Component	C_p [J/kg/K]	γ	Corresponding Air Temperature [K]
Diffuser	1005	1.4	260
LPC	1008	1.398	350
HPC	1099	1.354	800
Combustor	1216	1.313	1500
HPT	1190	1.318	1300
LPT	1142	1.335	1000
Core Exhaust	1029	1.387	500
Fan Exhaust	1005	1.4	273

A. Diffuser, Fan, and Compressor Model

Isentropic relations and a free stream Mach number, static pressure, and airspeed are used to constrain inlet stagnation quantities. When the engine model is used as part of a full aircraft optimization model, the ambient atmospheric properties and M_0 are linked to atmosphere and flight profile models. These values are set by the user if the engine is run in isolation. Diffuser boundary layer growth is neglected and a specified diffuser pressure ratio accounts for diffuser stagnation pressure drop. The constraints governing this are presented below. Z_0 replaces the non-GP compatible expression $1 + \frac{\gamma-1}{2}(M_0)^2$ in the stagnation relations.

$$\begin{aligned} a_0 &= \sqrt{\gamma R T_0} \\ u_0 &= M_0 a_0 \\ P_{t_0} &= P_0 {Z_0}^{3.5} \\ T_{t_0} &= T_0 Z_0 \\ h_{t_0} &= C_{p_{\text{air}}} T_{t_0} \\ P_{t_2} &= \pi_{\text{D}} P_{t_0} \\ T_{t_2} &= T_{t_0} \\ h_{t_2} &= h_{t_0} \end{aligned} \tag{7}$$

State change across the fan, low pressure compressor (LPC), and high pressure compressor (HPC) are computed using isentropic relations and user specified polytropic efficiencies.

$$\begin{aligned} P_{t_{i+1}} &= \pi_i P_{t_i} \\ T_{t_{i+1}} &= T_{t_i} \pi_i^{\frac{\gamma_i - 1}{\eta_i \gamma_i}} \\ h_{t_{i+1}} &= C_{p_i} T_{t_i} \end{aligned} \tag{8}$$

B. Combustor Model

The combustor constraints serve two purposes - to determine the fuel mass flow percentage and to account for the total pressure loss resulting from the mixing of the cooling flow and the working fluid in the main flow path. The flow mixing model is taken directly from TASOPT[4].

The fuel mass flow and T_{t_4} are constrained via an enthalpy balance (Equation 9) while Equations 10 and 11 determine the remaining station 4 states. η_{B} is the burner efficiency, a value less than one indicates a portion of injected fuel is not burned. The specified f_c is the cooling flow bypass ratio whose typical values range from 0.2-0.3, with lower values indicating a higher engine technology level. $C_{p_{\text{fuel}}}$ and h_{fuel} are taken as constants equal to 2010 J/kg/K and 43.003 MJ/kg respectively. $T_{t_{\text{f}}}$ is the fuel's temperature when injected into the combustor and π_{b} is the combustor pressure ratio. Both are user inputs.

$$\eta_{\text{B}} f_{\text{f}} h_{\text{fuel}} \geq (1 - f_c)(h_{t_4} - h_{t_3}) + C_{p_{\text{fuel}}} f_{\text{f}} (T_{t_4} - T_{t_{\text{f}}}) \tag{9}$$

$$h_{t_4} = C_{p_c} T_{t_4} \tag{10}$$

$$P_{t_4} = \pi_{\mathrm{b}} P_{t_3} \tag{11}$$

It is assumed the cooling flow is unregulated and engine pressure ratios are relatively constant so f_c will not change between operating points. Further, it is assumed the cooling flow mixes completely with the main flow between station 4a and the first row of turbine blades (station 4.1). The first row of turbine blades requires the majority of the cooling flow, justifying this assumption.

The mixed out flow temperature at station 4.1 is computed with the enthalpy balance in Equation 12. $f_{\mathrm{f+1}}$, given by equation 13, is used to make the term $f + 1$ GP compatible. This limits the total number of signomial constraints and makes the signomial constraints that do appear involve as few terms as possible. Both Equations 12 and 13 are signomial equalities.

$$h_{t_{4.1}} f_{\mathrm{f+1}} = (1 - f_c + f_{\mathrm{f}}) h_{t_4} + f_c h_{t_3} \tag{12}$$

$$f_{\mathrm{f+1}} = f_{\mathrm{f}} + 1 \tag{13}$$

The mixed-out state at station 4.1 is computed in terms of the temperature ratio Z4a, which is introduced for GP compatibility.

$$Z_{4a} = 1 + \frac{1}{2}(\gamma - 1)(M_{4a})^2 \tag{14}$$

$$P_{4a} = P_{t_4} (Z_{4a})^{-\frac{\gamma_i}{\gamma_i - 1}} \tag{15}$$

$$u_{4a} = M_{4a} \sqrt{\gamma_{4a} R T_{t_4} / Z_{4a}} \tag{16}$$

Cooling flow velocity, u_c, is defined by the user input cooling flow velocity ratio r_{uc}.

$$u_c = r_{\mathrm{uc}} u_{4a} \tag{17}$$

Static pressure rise during mixing is neglected and the station 4.1 state is computed using stagnation relations. Equation 19 is a signomial equality constraint.

$$P_{t_{4.1}} = P_{4a} \left(\frac{T_{t_{4.1}}}{T_{4.1}} \right)^{\frac{\gamma_i}{\gamma_i - 1}} \tag{18}$$

$$T_{4.1} = T_{t_{4.1}} - \frac{1}{2} \frac{{u_{4.1}}^2}{C_{p_c}} \tag{19}$$

Rather than introduce a full momentum balance, this model approximates $u_{4.1}$ as the geometric average of core and cooling flow velocities.

$$f_{\mathrm{f+1}} u_{4.1} = \sqrt{f_{\mathrm{f+1}} u_{4a} \alpha_{\mathrm{cool}} u_c} \tag{20}$$

C. Turbine Model

The low pressure turbine (LPT) must supply enough power to drive the fan and LPC. The high pressure turbine (HPT) must supply enough power to drive the HPC. This is ensured by enforcing the two shaft power balance constraints below, both of which are signomial equalities. $\bar{f}_o$ is equal to one minus the percent of mass flow bled to provide pressurization and deice (1-$\dot{m}_{offtake}/\dot{m}_{core}$). Shaft power offtakes for customer power are smeared into the shaft power transmission efficiencies, $\eta_{\mathrm{HP/LP}}$.

$$\bar{f}_o \eta_{\mathrm{HP}}(1+f_{\mathrm{f}})(h_{t_{4.1}} - h_{t_{4.5}}) = (h_{t_3} - h_{t_{2.5}}), \tag{21}$$

$$\bar{f}_o \eta_{\mathrm{LP}}(1+f_{\mathrm{f}})(h_{t_{4.9}} - h_{t_{4.5}}) = \alpha_{+1}(h_{t_{2.1}} - h_{t_2}) + (h_{t_{1.8}} - h_{t_{2.5}}), \tag{22}$$

The isentropic relations and user specified component polytropic efficiencies determine fluid states at stations 4.5 and 4.9.

$$P_{t_{i+1}} = \pi_i P_{t_i} \tag{23}$$

$$\pi_i = \left(\frac{T_{t_{i+1}}}{T_{t_i}}\right)^{\frac{\eta_i \gamma_i}{\gamma_i - 1}} \tag{24}$$

$$h_{t_{i+1}} = C_{p_i} T_{t_i} \tag{25}$$

D. Exhaust State Model

Thrust is determined with a momentum balance. Station 6 (core exhaust) and 8 (fan exhaust) velocities are computed by equations 26 to 29 which employ the stagnation relations and assume isentropic flow expansion.

$$\left(\frac{P_i}{P_{t_i}}\right)^{\frac{\gamma_i - 1}{\gamma_i}} = \frac{T_i}{T_{t_i}} \tag{26}$$

$$h_{t_i} = C_{p_i} T_{t_i} \tag{27}$$

$$h_i = C_{p_i} T_i \tag{28}$$

$$u_i{}^2 + 2h_i \leq 2h_{t_i} \tag{29}$$

Fan and core thrust (F_8 and F_6) are computed with a momentum balance and summed to set the total thrust.

$$F_8/(\alpha \dot{m}_{\mathrm{core}}) + u_0 \leq u_8 \tag{30}$$

$$F_6/(\bar{f}_o \dot{m}_{\mathrm{core}}) + u_0 \leq u_6 \tag{31}$$

$$F \leq F_6 + F_8 \tag{32}$$

The specific thrust, specific impulse, and corresponding thrust specific fuel consumption then follow.

$$F_{\text{sp}} = F/(a_0 \alpha_{+1} \dot{m}_{\text{core}}) \tag{33}$$

$$I_{\text{sp}} = \frac{F_{\text{sp}} a_0 \alpha_{+1}}{f_{\text{f}} g} \tag{34}$$

$$\text{TSFC} = \frac{1}{I_{\text{sp}}} \tag{35}$$

E. Engine Weight

In an aircraft optimization problem there is a downward pressure on engine weight. Consequently, the TASOPT[4] engine weight model can be relaxed into a posynomial inequality constraint. The TASOPT engine model is a fit to production engine data and does not account for the weight of a gearbox in a geared turbofan. The GP compatible engine weight constraint, taken from TASOPT[4], is presented below. $\dot{m}_{\text{total}}$ is defined by Equation 37 and α_{+1} is defined by Equation 38.

$$W \geq \frac{\dot{m}_{\text{core}} \dot{m}_{\text{total}}}{(100\text{lbm}) \dot{m}_{\text{core}} \alpha_{+1}} \left(1684.5 \text{ lbm } + 17.7 \text{ lbm } \frac{\pi_{\text{f}} \pi_{\text{LPC}} \pi_{\text{HPC}}}{30} + 1662.2 \text{ lbm } \left(\frac{\alpha}{5} \right)^{1.2} \right) \tag{36}$$

$\dot{m}_{\text{core}}$ is written in the equivalent form $\dot{m}_{\text{core}} \dot{m}_{\text{total}}/(\dot{m}_{\text{core}} \alpha_{+1})$ so an increase in either core or fan mass flow corresponds to an increase in engine weight, placing required downward pressure on both mass flows.

$$\dot{m}_{\text{total}} \geq \dot{m}_{\text{core}} + \dot{m}_{\text{fan}} \tag{37}$$

Equation 38 is a signomial equality constraint used for the same reasons as the constraint on $f_{\text{f}+1}$, discussed in Section IV B. There is an upward pressure on α (engines with a larger by-pass ratio tend to be more efficient) and α_{+1} due to equations 34 and 35, so the GP compatible posynomial inequality $\alpha_{+1} \geq \alpha + 1$ would not remain tight.

$$\alpha_{+1} = \alpha + 1 \tag{38}$$

F. Area, Mass Flow, and Speed Constraints

Either the engine's thrust or the turbine inlet temperature must be constrained via Equation 39 or 40. In a full aircraft optimization problem, F_{spec} can be linked to thrust requirements in an aircraft performance model. When the engine model is run in isolation, F_{spec} or $T_{t_{4.1}}$ must be specified by the user.

$$F = F_{\text{spec}} \tag{39}$$

$$T_{t_{4.1}} = T_{t_{4_{\text{spec}}}} \tag{40}$$

Component speed ratios are determined by the turbo-machinery maps (section IV G). Only the ratio of component speed to the component's nominal design speed is considered, so the nominal design speed is arbitrarily set to one. Thus, an LPC speed of $N_1 = 1.1$ should be thought of as an LPC speed 10 percent faster than the components nominal design speed, not a value 10 percent over max RPM. This model does not attempt to constrain actual RPM values.

The fan and LPC both lie on the low pressure shaft so their speeds are correlated via Equation 41, which allows for a user selected gearing ratio G_{f}. Additionally, a maximum allowable speed is set for the fan and compressors. The max speed of 1.1 is estimated from TASOPT output. If an upper bound is not placed on speed, the optimizer will indefinitely increase component speed to drive OPR higher. When solving across an engine mission profile, the upper speed bound will only be achieved at the engine's most demanding operating point.

$$N_{\mathrm{f}} = G_{\mathrm{f}} N_1 \tag{41}$$

$$N_1 \leq 1.1 \tag{42}$$

$$N_2 \leq 1.1 \tag{43}$$

Constraints on the mass flux through engine components are used to ensure each engine operating point corresponds to an engine of the same physical size. The station 5 and 7 exit states are determined using user specified nozzle pressure ratios as well as isentropic and stagnation relations.

$$P_{t_5} = \pi_{\mathrm{tn}} P_{t_{4.9}} \tag{44}$$

$$P_{t_7} = \pi_{\mathrm{fn}} P_{t_2} \tag{45}$$

$$P_i \geq P_0 \tag{46}$$

$$\frac{P_i}{P_{t_i}} = \left(\frac{T_i}{T_{t_i}}\right)^{\frac{\gamma}{\gamma-1}} \tag{47}$$

$$\left(\frac{T_i}{T_{t_i}}\right)^{-1} \geq 1 + 0.2(M_i)^2 \tag{48}$$

Equation 49 is a deviation from constraints in traditional engine models that use Newton's method or a comparable iterative procedure. In many methods, M_5 and M_7 are set equal to 1 if M_6 or M_8 is respectively greater than 1 so that the exit nozzle is choked. If M_6 or M_8 is less than 1, then M_5 and M_7 are constrained to be less than 1. A switch is used to change constraints mid solve. It is not possible to switch constraints during a GP solve. Therefore, M_5 and M_7 are constrained to be less than or equal to 1, regardless of M_6 and M_8. For the mild choking typical in efficient turbofans, the effects of this reformulation are negligible, as confirmed by section V.

$$M_i \leq 1 \tag{49}$$

The constraint on u_i in equation 50 ensures reverse flow does not occur.

$$u_i \geq u_0 \tag{50}$$

Equations 51 to 62 set A_2, $A_2.5$, A_5, and A_7. Note $M_{2.5}$ is set by the user and M_2 is either linked to an aircraft performance model or set by the user.

$$a_i = \sqrt{\gamma R T_i} \tag{51}$$

$$u_i = a_i M_i \tag{52}$$

$$\rho_i = \frac{P_i}{R T_i} \tag{53}$$

In the static property calculations, the temperature ratio Z_i is again introduced for GP compatibility.

$$Z_i = 1 + \frac{\gamma_i - 1}{2} {M_i}^2 \tag{54}$$

$$P_i = P_{t_i} (Z_i)^{\frac{\gamma}{1-\gamma}} \tag{55}$$

$$T_i = T_{t_i} Z_i^{-1} \tag{56}$$

$$h_i = C_{p_i} T_i \tag{57}$$

$$\rho_i = P_i / (R T_i) \tag{58}$$

In equation 59, the value of $C_{p_i} - R$ is precomputed and substituted into the constraint to make it GP compatible.

$$u_i = M_i \sqrt{C_{p_i} R T_i / (C_{p_i} - R))} \tag{59}$$

$$\dot{m}_{\text{fan}} = \rho_7 A_7 u_7 \tag{60}$$

$$\dot{m}_{\text{core}} \bar{f}_o = \rho_5 A_5 u_5 / f_{\text{f+1}} \tag{61}$$

$$\alpha = \dot{m}_{\text{fan}} / \dot{m}_{\text{core}} \tag{62}$$

Full turbine maps are not used to constrain turbine mass flow. Instead, it is assumed the entry to each turbine is always choked. This leads to two constraints, each setting the corrected mass flow at turbine entry equal to the estimated nominal value.

$$\bar{m}_{\mathrm{HPT}_D} = \bar{m}_{\mathrm{HPC}} f_{\mathrm{f+1}} \bar{f}_o (P_{t_{2.5}}/P_{t_{4.1}}) \sqrt{T_{t_{4.1}}/T_{t_{2.5}}} \tag{63}$$

$$\bar{m}_{\mathrm{LPT}_D} = \bar{m}_{\mathrm{LPC}} f_{\mathrm{f+1}} \bar{f}_o (P_{t_{1.8}}/P_{t_{4.5}}) \sqrt{T_{t_{4.5}}/T_{t_{1.8}}} \tag{64}$$

The optimized nominal core mass flow is computed via equation 65. $\hat{T}_i$ and $\hat{P}_i$ represent the estimated nominal state at engine station i. The values of $\hat{T}_{t_4}$, $\hat{P}_{t_2}$, and $\hat{T}_{t_2}$ are set by the user while all other $\hat{T}$ and $\hat{P}$ values are estimated using the isentropic relations, component design pressure ratios, and a shaft power balance. This process is shown in equation set 66. Nominal mass flows are allowed to vary plus or minus 30 percent from their estimated values to account for uncertainty in the estimation process and ensure that if the nominal design condition is estimated to occur at the aircraft's average altitude, the optimizer can place the nominal state anywhere in the flight. Optimization of the nominal state enables removal of the apriori specification of an engine on-design point.

$$\begin{aligned} \bar{m}_{\mathrm{component}_D} &\leq 1.2 f_{\mathrm{f+1}} \bar{f}_o \dot{m}_{\mathrm{core_D}} \sqrt{\hat{T}_{t_i}/T_{\mathrm{ref}}}/(\hat{P}_{t_i}/P_{\mathrm{ref}}) \\ \bar{m}_{\mathrm{component}_D} &\geq 0.8 f_{\mathrm{f+1}} m_{\mathrm{off}} \dot{m}_{\mathrm{core_D}} \sqrt{\hat{T}_{t_i}/T_{\mathrm{ref}}}/(\hat{P}_{t_i}/P_{\mathrm{ref}}) \end{aligned} \tag{65}$$

$$\begin{aligned} \hat{P}_i &= \pi_{\mathrm{component}} \hat{P}_{i-1} \\ \hat{T}_{t_i} &= \hat{T}_{t_{i-1}} (\pi_{\mathrm{component}})^{\frac{\gamma-1}{\gamma \eta_i}} \\ \hat{T}_{t_{4.5}} &= \hat{T}_{t_{4.1}} - (\hat{T}_{t_3} - \hat{T}_{t_{2.5}}) \\ \hat{T}_{t_{4.9}} &= \hat{T}_{t_{4.5}} - (\hat{T}_{t_{2.5}} - \hat{T}_{t_{2.1}}) \\ \hat{\pi}_{\mathrm{HPT}} &= \left(\frac{\hat{T}_{t_{4.5}}}{\hat{T}_{t_{4.1}}} \right)^{\frac{\eta_s \gamma}{\gamma-1}} \\ \hat{P}_{t_{4.5}} &= \hat{\pi}_{\mathrm{HPT}} \hat{P}_{t_3} \end{aligned} \tag{66}$$

G. Fan and Compressor Maps

Fan and compressor maps are required to accurately constrain fan and compressor pressure ratios. Every engine has different compressor maps that result from detailed turbo-machinery design. The present model does not attempt to take into account factors causing variations in turbo-machinery maps. Instead, a simple compressor and fan map is assumed and applied to all engines. As argued in section V, this is accurate enough for aircraft conceptual design optimization.

GP compatible fan and compressor maps were derived from NASA's Energy Efficient Engine (E3) program[13] turbomachinery maps, which are presented in Figures 5 and 6. These are also the maps used in TASOPT. Blue curves are lines of constant component speed and red curves are the estimated engine operating line, or spine. Each spine can be parametrized as either $\pi = f(\bar{m})$ or $\pi = f(N)$, where $\bar{m}$ is normalized corrected mass flow and N is component speed. The normalized corrected mass for for each components is defined below.

$$\bar{m}_{\mathrm{HPC}} = \dot{m}_{\mathrm{core}} \sqrt{T_{2.5}/T_{\mathrm{ref}}}/(P_{t_{2.5}}/P_{\mathrm{ref}}) \tag{67}$$

$$\bar{m}_{\mathrm{LPC}} = \dot{m}_{\mathrm{core}} \sqrt{T_2/T_{\mathrm{ref}}}/(P_{t_2}/P_{\mathrm{ref}}) \tag{68}$$

$$\bar{m}_{\mathrm{fan}} = \dot{m}_{\mathrm{fan}} \sqrt{T_2/T_{\mathrm{ref}}}/(P_{t_2}/P_{\mathrm{ref}}) \tag{69}$$

A GP compatible monomial approximation to the functions $\pi = f(\bar{m})$ and $\pi = f(N)$ was developed with GPfit[14, 15]. The approximations for both the compressor and fan map spine fits are given by Equations 70 through 73 and plotted in Figures 7 and 8.

$$\pi_{\text{comp}} = 20.1066(N)^{5.66} \tag{70}$$

$$\pi_{\text{comp}} = 25.049(\bar{m})^{1.22} \tag{71}$$

$$\pi_{\text{fan}} = 1.6289(N_{\text{f}})^{0.871} \tag{72}$$

$$\pi_{\text{fan}} = 1.7908(\bar{m})^{1.37} \tag{73}$$

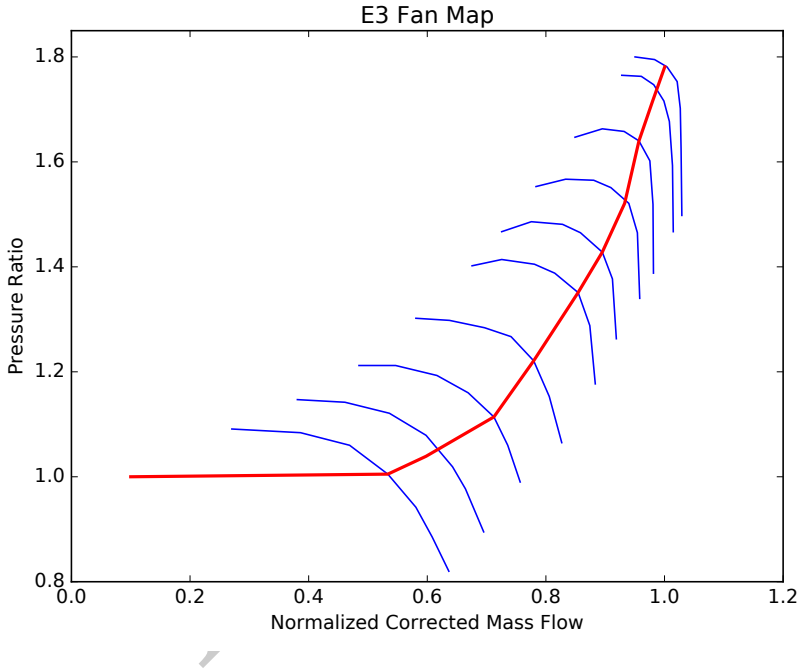

Fig. 5 E3 fan map with an estimated engine operating line in red. The map's design pressure ratio is 1.7.

The fan map spine was only fit for speeds greater than 0.6. Single term fits are monomials that must pass through the origin, limiting their ability to capture fan trends for low speeds. During a typical flight, the low pressure spool speed (N_1) will rarely, if ever, drop below 0.6. The fitted map, combined with the constraint all pressure ratios are greater than 1, places an implicit lower bound on N_1 and N_{f} which may lead to modeling inaccuracy at low throttle settings. This is acceptable due to the proportionally small amount of fuel burned at low throttle settings. A two term polynomial fit yields a better approximation of the fan map, but was not used because it adds an additional signomial constraint.

Equations 74 through 76 are fan and compressor map approximations obtained by scaling the E3 map fits to an arbitrary user specified design pressure ratio and constraining the pressure ratio be within 10 percent of the spine mass flow fit. This allows the operating point to move off the operating line while ensuring the operating point does not move into either the stall or surge regime. The user

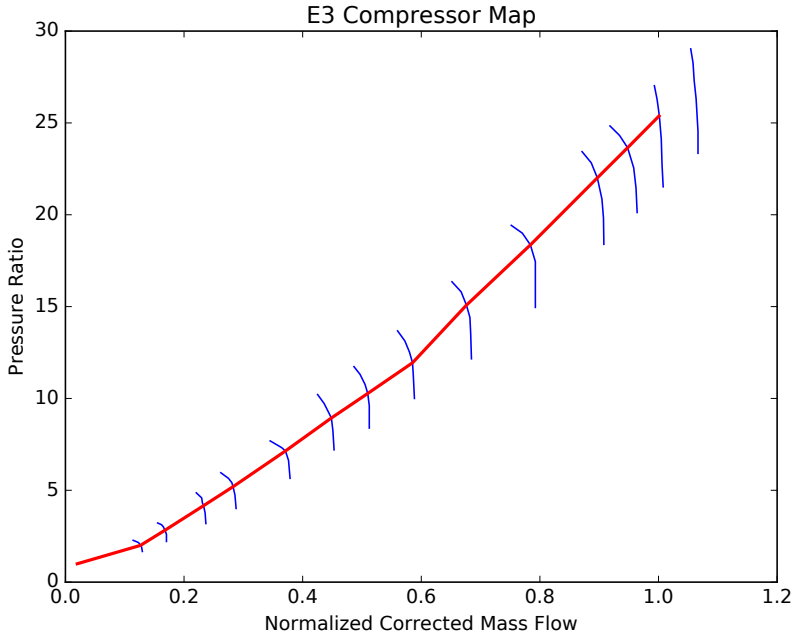

Fig. 6 E3 compressor map with an estimated engine operating line in red. The map's design pressure ratio is 26.

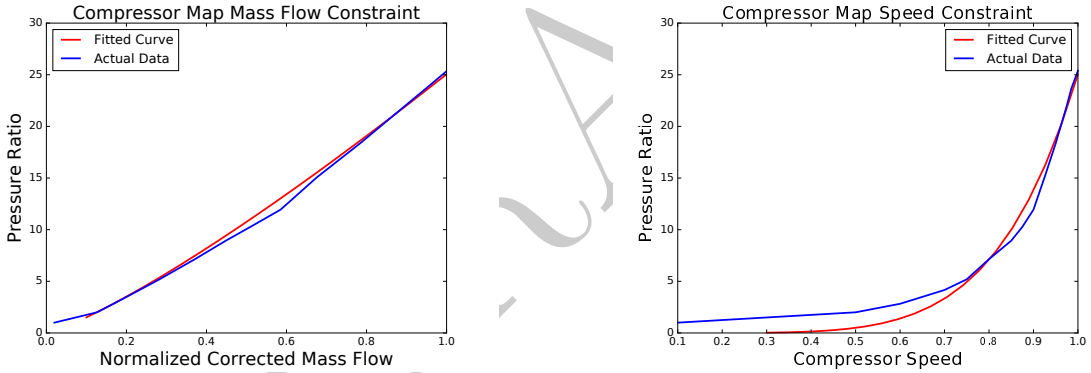

(a) Mass flow parametrization

(b) Speed parametrization

Fig. 7 Monomial approximations to the E3 compressor map spine.

must specify fan, LPC, and HPC design pressure ratios. Setting these values partially determines the map constraints and is distinct from specifying a full engine on-design operating point. If the fan and compressor design pressure ratios were left free, the optimizer would push them to infinity.

$$\begin{aligned}
\pi_{\text{fan}}\left(\frac{1.7}{\pi_{\text{f}_\text{D}}}\right) &= 1.6289(N_\text{f})^{0.871} \\
\pi_{\text{fan}}\left(\frac{1.7}{\pi_{\text{f}_\text{D}}}\right) &\geq (0.95)1.7908(\bar{m}_f)^{1.37} \\
\pi_{\text{fan}}\left(\frac{1.7}{\pi_{\text{f}_\text{D}}}\right) &\leq (1.05)1.7908(\bar{m}_f)^{1.37}
\end{aligned} \tag{74}$$

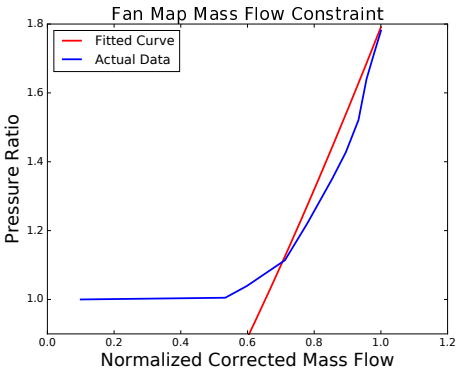

(a) Mass flow parametrization

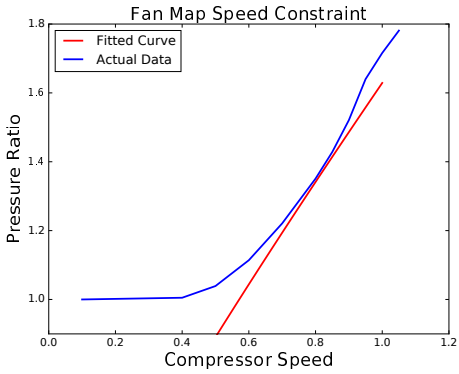

(b) Speed parametrization

Fig. 8 Monomial approximations to the E3 fan map spine.

$$\begin{aligned}
\pi_{\mathrm{LPC}}\left(\frac{26}{\pi_{\mathrm{LPC_D}}}\right) &= 20.1066(N_1)^{5.66} \\
\pi_{\mathrm{LPC}}\left(\frac{26}{\pi_{rmLPC_D}}\right) &\geq (0.95)25.049(\bar{m}_{\mathrm{LPC}})^{1.22} \\
\pi_{\mathrm{LPC}}\left(\frac{26}{\pi_{rmLPC_D}}\right) &\leq (1.05)25.049(\bar{m}_{\mathrm{LPC}})^{1.22}
\end{aligned} \tag{75}$$

$$\begin{aligned}
\pi_{\mathrm{HPC}}\left(\frac{26}{\pi_{\mathrm{HPC_D}}}\right) &= 20.1066(N_2)^{5.66} \\
\pi_{\mathrm{HPC}}\left(\frac{26}{\pi_{\mathrm{HPC_D}}}\right) &\geq (0.95)25.049(\bar{m}_{\mathrm{HPC}})^{1.22} \\
\pi_{\mathrm{HPC}}\left(\frac{26}{\pi_{\mathrm{HPC_D}}}\right) &\leq (1.05)25.049(\bar{m}_{\mathrm{HPC}})^{1.22}
\end{aligned} \tag{76}$$

It is possible to fit a full compressor map instead of just the spine. However, there is no way to distinguish valid map points from points in the surge/stall regime. The optimizer will push the operating point towards these sections of the map, resulting in a physically invalid solution.

V. Model Validation

The presented model was validated against the output of a CFM56-7B27 like NPSS model, a GE90-94B like NPSS model, and TASOPT. The NPSS models were developed by Georgia Tech with publicly available data under the FAA's Environmental Design Space effort[16]. The NPSS output was provided by NASA. The TASOPT data was taken from a 737-800 optimization run. The TASOPT engine output should mirror that of NASA's CFM56 like model because the CFM56-7B family powers all 737 Next Gen aircraft[17]. The intent of the validation studies was to verify the model's physics modeling, not to find the most optimal engine. Essentially, during validation the model was used for engine analysis instead of optimization.

During validation, the objective function was the sum of all climb TSFCs plus ten times the cruise TSFC multiplied by engine weight raised to the 0.00001 (equation 77). Cruise TSFC was weighted by a factor of ten to capture the fact that a commercial aircraft spends the majority of each flight in cruise. The small engine weight term was included to prevent engine mass flow from growing without bound. To prevent engine size from growing without bound, BPR was constrained to be less than the validation data's max BPR.

The model's output is not sensitive to the value of the weight exponent so long as it is small. Solving the baseline CFM 56 validation case (section V 1) with a weight exponent of 0.00001 yields

Table 2 Input values used in all three validation cases.

Variable	Value	Units
T_{t_f}	435	K
$C_{p_{4.1}}$	1.280	KJ/kg/K
$C_{p_{4.5}}$	1.184	KJ/kg/K

Table 3 The number of GP solves and solution time for each validation case.

Validation Case	Number of GP solves	Solution Time [s]
CFM56	9	5.73
TASOPT	6	3.31
GE90	10	4.34

TSFCs of 0.633519 and 0.64310. Decreasing the exponent to 0.001 and resolving yields TSFCs of 0.633512 and 0.643126, a difference of 0.001 and 0.003 percent respectively.

Component polytropic efficiencies, duct pressure losses, cooling flow bypass ratio, and max BPR are estimated from TASOPT/NPSS output. To mitigate errors due to the SP model's assumed gas properties, TASOPT computed turbine C_p values were used in all three validation cases (NPSS computed C_p was not available in the provided output). These values, along with the assumed fuel temperature, are presented in Table 2.

Validation solution speeds are presented in Table 3.

$$\text{objective} = \left(\frac{W_{\text{engine}}}{1\text{N}}\right)^{0.0001} \left(\sum \text{TSFC}_{\text{climb}} + 10\,\text{TSFC}_{\text{cruise}}\right) \tag{77}$$

1. NPSS CFM56 Validation

The SP model's input values are given in Table 4. The SP model was constrained by two operating points, on-design and TOC, detailed in Table 5. The cruise and TOC operating points have similar ambient conditions and thrust requirements, so the SP model should place the on-design point near the NPSS on-design point, producing little variation in predicted TSFC. Validation results are given in Table 6.

The SP turbofan model was solved for two different h_f values. Typically, the SP model has an h_f of 43.003 MJ/kg. However, NASA's NPSS model has an implied h_f value of 40.8 MJ/kg, 5.12 percent less than SP model's value and 2 MJ/kg below the minimum h_f of Jet A[18]. Solving the SP model with an h_f of 40.8 MJ/kg reduces the percent error at each operating point by approximately 5 percent. The remaining error can be accounted for by variations in component maps and gas properties.

Table 4 Input values used for CFM56 engine validation.

Variable	Value	Variable	Value
π_{f_D}	1.685	$\alpha_{\max}$	5.105
$\pi_{\text{LPC}_\text{D}}$	1.935	f_c	0.19036
$\pi_{\text{HPC}_\text{D}}$	9.369	η_{fan}	0.9005
η_{B}	0.9827	η_{LPC}	0.9306
G_{f}	1	η_{HPC}	0.9030
$\bar{f}_o$	0.9556	η_{HPT}	0.9030
η_{LPT}	0.8851	η_{HP}, η_{LP}	0.97
π_{tn}	0.98	π_{b}	0.94
π_{D}	0.98	π_{fn}	0.98

Table 5 The two operating points used during CFM56 validation.

Flight Condition	Altitude [ft]	Mach Number	Thrust [lbf]
TOC	35,000	0.8	5,961.9
On-Design (cruise)	35,000	0.8	5,496.4

Table 6 NPSS CFM56 validation results, expected to be similar when h_f = 40.8 MJ/kg.

Flight Condition	Predicted TSFC [1/hr]	NPSS TSFC [1/hr]	Percent Difference
On Design (SP h_f = 43.003 MJ/kg)	0.6335	0.6793	-6.74
On Design (SP h_f = 40.8 MJ/kg)	**0.6679**	**0.6793**	**-1.67**
Top of Climb (SP h_f = 43.003 MJ/kg)	0.6431	0.6941	-7.34
Top of Climb (SP h_f = 40.8 MJ/kg)	**0.6679**	**0.6941**	**-2.32**
TASOPT On-Design (implied h_f = 42.68 MJ/kg)	0.63403	0.6941	-6.66
Engine Weight (SP h_f = 43.003 MJ/kg)	21,016.84 N	23,201.92 N	-9.42
Engine Weight (SP h_f = 40.8 MJ/kg)	21,039.71 N	23,201.92 N	-9.32

2. TASOPT Validation

The SP turbofan model was validated against three TASOPT operating points: take-off, TOC, and on-design. The parameters for each operating point are given in Table 7. The constant input values are given in Table 8. Validation results are presented in Table 9.

The SP model's engine was optimized to meet conditions at 35,000 feet. The fan inlet area is 1.51 percent smaller than TASOPT's fan area while the fan exhaust area is 46.33 percent larger than TASOPT's. This permits greater flow expansion and pressure matching at altitude but degrades climb performance. This works objective function, Equation 77, estimates how climb and cruise fuel burn are weighted. TASOPT is a full system optimization code which more accurately weights climb/cruise fuel. This is expected and creates a discrepancy. This work's assumed fan map is a second source of discrepancy. As discussed in section IV G, the fan SP model's fan map is conservative, particularly for high fan speeds. At TOC, the low pressure spool is at its max allowed speed of 1.1. The SP model predicts a fan pressure ratio of 1.75 while TASOPT has a fan pressure ratio of 1.8709, 6.46 percent higher. The lower FPR causes the engine to produce more core thrust, lowering efficiency and increasing TSFC.

The relatively small errors between the presented model and TASOPT validate the presented model's method of simulating an engine without specifying an on-design point.

3. NPSS GE90 Validation

The two operating points used for GE90 validation are given in Table 10. Again, TOC conditions are similar to cruise conditions, so TSFC discrepancies should be small. The SP model's input values are given in Table 11.

There is a larger TSFC discrepancy in this validation case than the NPSS CFM56 validation case for two reasons. TASOPT (effectively 737 CFM56) hot section C_p values are used. The NPSS GE90 implied C_p values are unknown, but it is reasonable to assume they deviate from TASOPT's 737 values. Additionally, the NPSS model has component maps more appropriate for the larger engine. This validation case nevertheless demonstrates that the presented model accurately scales from a CFM56 up to a GE90.

Table 7 The three operating points used when validating the presented model against TASOPT.

Flight Condition	Altitude [ft]	Mach Number	Thrust [lbf]
Take-Off	0	0.223	21,350
TOC	35,000	0.8	6,768
On-Design (cruise)	35,000	0.8	4,986

Table 8 Input values used for TASOPT and CFM56 engine validation.

Variable	Value	Variable	Value
π_{f_D}	1.685	α_{max}	5.105
π_{LPC_D}	4.744	f_c	0.19036
π_{HPC_D}	3.75	η_{fan}	0.8948
η_B	0.9827	η_{LPC}	0.88
G_f	1	η_{HPC}	0.87
$\bar{f}_o$	0.9556	η_{HPT}	0.899
η_{LPT}	0.889	η_{HP}, η_{LP}	0.97
π_{tn}	0.989	π_b	0.94
π_D	0.998	π_{fn}	0.98

Table 9 TASOPT validation results, expected to be similar at on design.

Flight Condition	Predicted TSFC [1/hr]	TASOPT TSFC [1/hr]	Percent Difference
Takeoff	0.5334	0.48434	10.13
Top of Climb	0.6750	0.65290	3.39
On Design (cruise)	**0.6359**	**0.64009**	**-0.66**
Engine Weight	37,540.76 N	35,010.62	7.23

VI. Optimum-Aircraft Parametric Studies

The engine model was integrated with a simplified commercial aircraft sizing model and the combined models were solved to find the aircraft/engine combination that burns the least amount of fuel. The model was solved with a variety of flight profiles as well as a varying number of missions, mission ranges, and minimum climb rates. Effects of these changes on engine sizing and parameter sensitivities are presented. The commercial aircraft sizing model is intentionally simple, capturing only general trends in aircraft sizing. A detailed description of the commercial sizing model is available in Appendix A. For the purposes of this paper, each mission was discretized into four flight segments - two climb and two cruise. The objective is to minimize total fuel burn. Table 13 lists the input values given to the aircraft model. The same engine input values are used as during CFM56 validation (Table 4). The integrated engine/commercial aircraft sizing model has 628 free variables and solves in 6.78 seconds (6 GP iterations).

A. Optimum-Aircraft Sensitivity to Specified Mission Range

To demonstrate that the combined model captures the proper trends, it was solved for a variety of mission ranges. Each point on the following plots represents a unique aircraft/engine combination. Total fuel burn increased with range, as shown by Figure 9.

Figure 10 presents plots of max engine thrust, fan and core thrust, initial climb and cruise TSFC, and engine weight versus mission range. All values remain roughly constant across mission range.

B. Optimum-Aircraft Sensitivity to Specified Minimum Climb Rate

A minimum initial climb rate constraint was added to shift the nominal design point towards climb. The minimum climb rate was for normal operating conditions (i.e. both engines operating nominally). Increasing the minimum initial climb rate creates a need for increased thrust at low

Table 10 The two operating points used when validating the presented model against the GE90 like NPSS model.

Flight Condition	Altitude [ft]	Mach Number	Thrust [lbf]
TOC	35,000	0.85	19,600
On-Design (cruise)	35,000	0.8	16,408.4

Table 11 Input values used for GE90 engine validation

Variable	Value	Variable	Value
π_{f_D}	1.58	α_{max}	8.7877
π_{LPC_D}	1.26	f_c	0.1444
π_{HPC_D}	20.033	η_{fan}	0.9153
η_B	0.997	η_{LPC}	0.9037
G_f	1	η_{HPC}	0.9247
$\bar{f}_o$	0.97	η_{HPT}	0.9121
η_{LPT}	0.9228	η_{HP}, η_{LP}	0.98
π_{tn}	0.98	π_b	0.94
π_D	0.98	π_{fn}	0.98

Table 12 NPSS GE90 validation results, expected to be similar at both operating points.

Flight Condition	Predicted TSFC [1/hr]	NPSS TSFC [1/hr]	Percent Difference
On Design	0.5631	0.5418	2.21
TOC	0.5973	0.5846	3.92
Engine Weight	73,270.54 N	77,399.06 N	-5.33

altitude, similar to adding a minimum balanced field length requirement to an aircraft. The aircraft model was solved across a range of minimum climb rates.

The initial thrust requirement on the engine was larger the higher the minimum climb rate. This is presented in Figure 11. Note the minimum climb rate constraint does not become active until the minimum climb rate exceeds 1,317 ft/min. The total thrust, fan thrust, and core thrust (also plotted in Figure 11) all increase in a near linear manner.

The engine model predicts engine weight will increase with minimum rate of climb, as shown in Figure 12. This is the same as saying engine weight will increase with thrust, which is expected.

As the engine is required to produce more thrust it gets physically larger. Figure 13 illustrates this with a plot of fan area versus minimum initial climb rate.

Figure 14 presents the initial climb and cruise TSFC versus the minimum initial climb rate. For low minimum initial climb rates, the nominal design point remained at cruise and the cruise TSFC was virtually unaffected by the higher climb rate. However, as the climb rate continued to increase, the design point shifted toward climb and cruise TSFC began to increase. Essentially, the high minimum climb rate requirement is degrading cruise performance. A short balanced field length requirement would degrade the performance of a commercial aircraft in a similar way.

C. Full Mission Versus Cruise Only Optimization

To illustrate how the removal of the on/off design point distinction allows this paper's engine model to select the optimal engine, the climb portion of the flight was removed and the optimal cruise engine was compared to the full mission optimal engine. The aircraft in both missions had the same fuselage area, carried the same payload, and had a cruise range of 2,000 nm. Results are presented in Table 14. The nominal design point is shifted towards climb for the full mission engine, causing it to burn 3.5 percent more fuel during cruise than the cruise only engine. All component areas are larger on the cruise only engine, which is (surprisingly) also 43 percent lighter. When climb

Table 13 Aircraft sizing and flight profile inputs.

Variable	Value	Unit
N_{eng}	2	-
$W_{S_{max}}$	6,664	N/m^2
N_{pax}	150	-
e	0.9	
AR_{max}	10	-

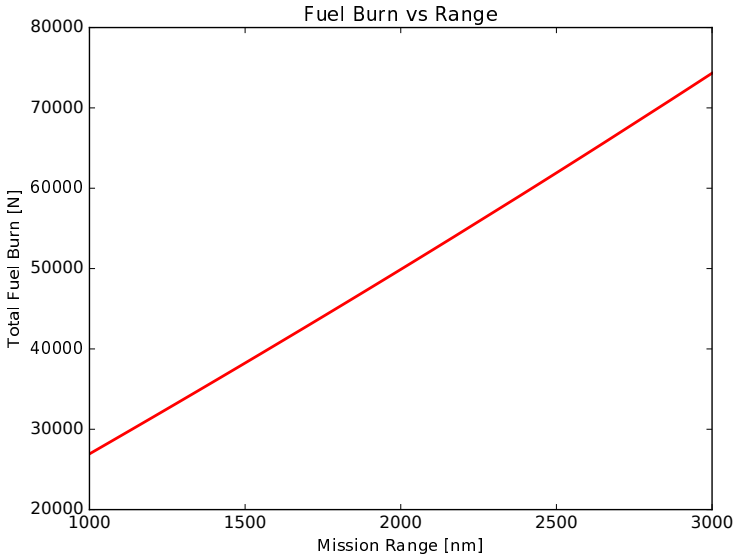

Fig. 9 Total fuel burn versus mission range.

Table 14 Differences in engine size when accounting for the full mission profile and just cruise.

Variable	Full Mission Value	Cruise Only Value	Percent Difference
A_2	0.622 m^2	0.751 m^2	-20.76
A_5	0.158 m^2	0.180 m^2	-12.20
A_7	0.383 m^2	0.458 m^2	-19.57
Engine Weight	10,714.62 N	6,062.41 N	43.42
Initial Cruise TSFC	0.400 1/hr	0.402 1/hr	-2.12

is not considered, the max thrust requirement and mass flow through the engine are substantially smaller. Consequently, the mass flow dependent data fit engine weight model (Equation 36) predicts an unrealistically light engine.

D. Multi-Mission Optimization

An extra layer of vectorization was added and the presented engine and simple aircraft model was simultaneously optimized across four missions of ranges 500 nm, 1,000 nm, 1,500 nm, and 2,000 nm. Commercial aircraft are designed for high mission flexibility which degrades overall fuel efficiency, motivating the use of multiple design reference missions when optimizing an aircraft[19]. For simplicity, payload remained constant for each mission. It is assumed the aircraft being optimized will fly 500 nm missions 37.5 percent of the time, 1,000 nm mission 37.5 percent of the time, 1,500 nm missions 12.5 percent of the time, and 2,000 nm missions 12.5 percent of the time. Equation 78 is the weighted objective function for this problem.

$$\text{objective} = 0.375W_{\text{fuel}_{500\text{nm}}} + 0.375W_{\text{fuel}_{1,000\text{nm}}} + 0.125W_{\text{fuel}_{1,500\text{nm}}} + 0.125W_{\text{fuel}_{2,000\text{nm}}} \tag{78}$$

Table 15 presents differences in the optimal engine size and fuel burn for the two optimizations. As expected, the multi-mission optimized aircraft burns more fuel during the 2,000 nm mission than the aircraft optimized for just the 2,000 nm flight.

The multi-mission optimization problem has 2,460 free variables and takes 28.3 seconds and six GP iterations to solve.

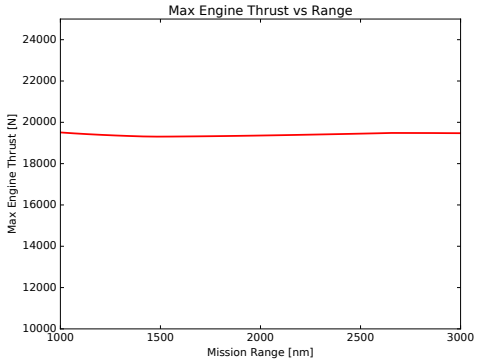

(a) Max engine thrust, which occurs during the initial climb segment, versus mission range.

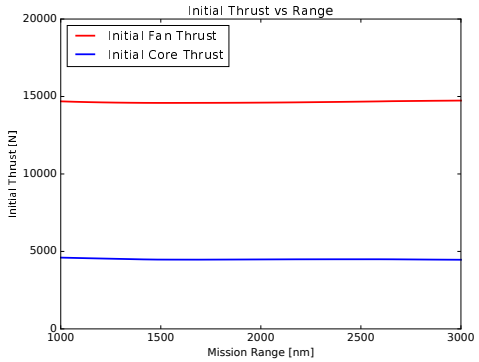

(b) Fan and core thrust during the initial climb segment versus mission range.

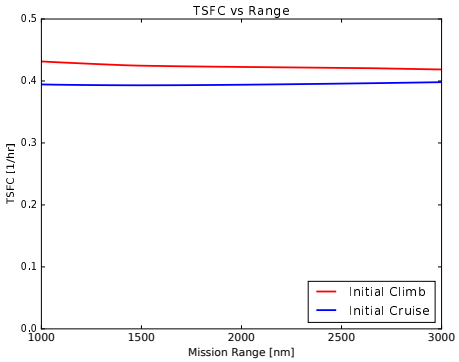

(c) Initial climb and cruise TSFC versus mission range

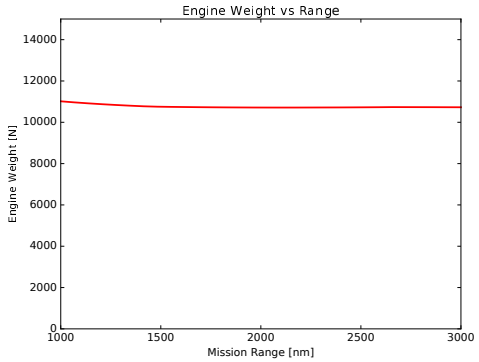

(d) Engine weight versus mission range.

Fig. 10 Initial engine thrust, core and fan thrust, climb and cruise TSFC, as well as engine weight for a variety of mission ranges.

Table 15 Differences in engine size for the presented multi-mission optimization formulation and a single 2,000 nm range mission optimization.

Variable	Single Mission Value	Multi-Mission Value	Percent Difference
A_2	0.622 m^2	0.617 m^2	0.77
A_5	0.158 m^2	0.160 m^2	-1.58
A_7	0.383 m^2	0.406 m^2	-5.79
Engine Weight	10,714.62 N	10,950.19 N	-2.20
2,000 nm Fuel Burn	43,3335.19 N	43,694.08 N	-0.83

E. Sensitivity Discussion

A strength of convex optimization is that, together with the optimum solution, it provides sensitivities of this solution to all model parameter values. Sensitivities are all local and computed about the optimal point. Equation 79[10] is the formula for parameter sensitivities. If the sensitivity to a constant is 0.5 then decreasing that constant by one percent will decrease the objective by approximately one half a percent. If the sensitivity to a constant is -0.75, then a one percent increase in the constant will decrease the objective by approximately three quarters of a percent. Analyzing a model's sensitivities can be useful in two ways. The first is to determine which areas of a physical design should be improved. For example, if the sensitivity to burner pressure drop is very large, it is advantageous to make the burner pressure drop as small as possible. The second way sensitivities can be used is to guide model development. If the sensitivity to a constant is low, it may not be worthwhile to develop an intricate model for that constant. However, if the sensitivity is large, it is important to ensure it is accurately modeled.

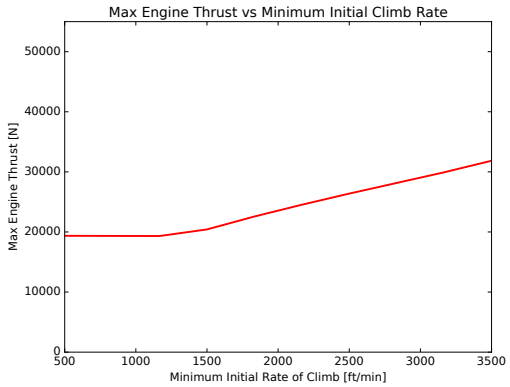

(a) Total initial thrust

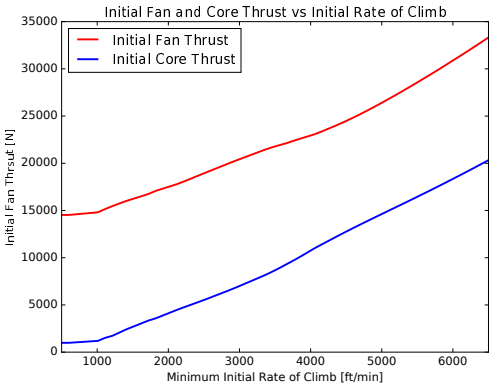

(b) Initial fan and core thrust

Fig. 11 Initial fan and core thrust versus minimum initial climb rate.

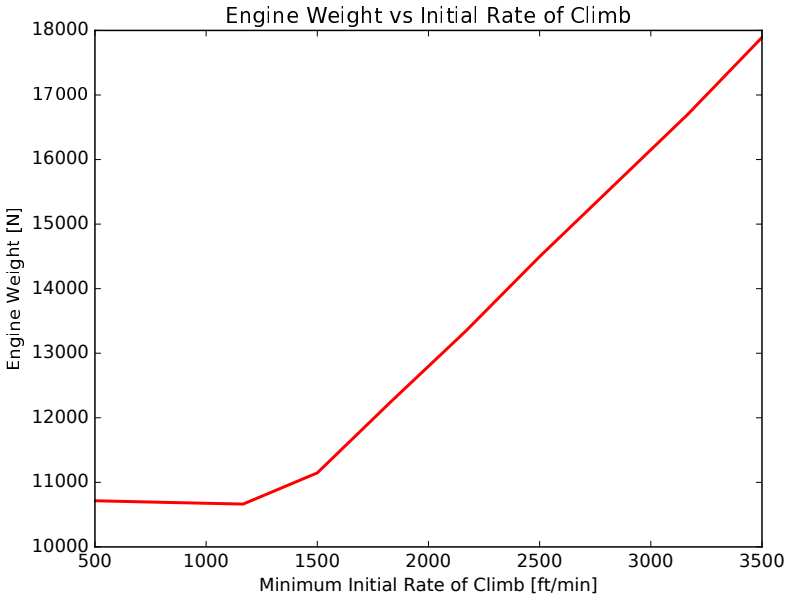

Fig. 12 Engine weight versus minimum initial climb rate.

$$\text{Parameter Sensitivity} = \frac{\text{Fractional Objective-Function Change}}{\text{Fractional Parameter Change}} \tag{79}$$

The integrated aircraft optimization problem was solved with a mission range of 2,000 nm. Table 16 presents some a subset of engine sensitivities. The solution is most sensitive to core bleed flow, HP shaft power transmission efficiency, diffuser pressure ratio, the combustor efficiency, and the fan duct pressure loss. Increasing any of these values will decrease fuel burn. There is a positive sensitivity to the fan design pressure ratio. Increasing the fan design pressure ratio will decrease fuel burn.

Table 17 presents sensitivities to some of the assumed constants in the aircraft model. Trends are as expected. Increasing the wing span and Oswald efficiency factor decreases fuel burn while decreasing passenger weight and mission range decreases fuel burn.

It is also interesting to analyze how sensitivities change as mission parameters change. Figure 15 is a plot of the sensitivity to the fan design pressure ratio versus minimum initial climb rate.

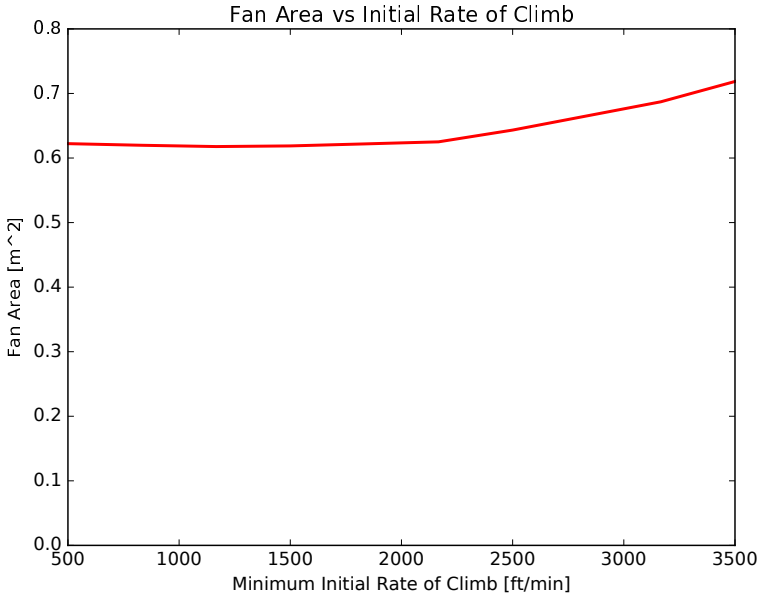

Fig. 13 Fan inlet area (A_2) versus minimum initial climb rate.

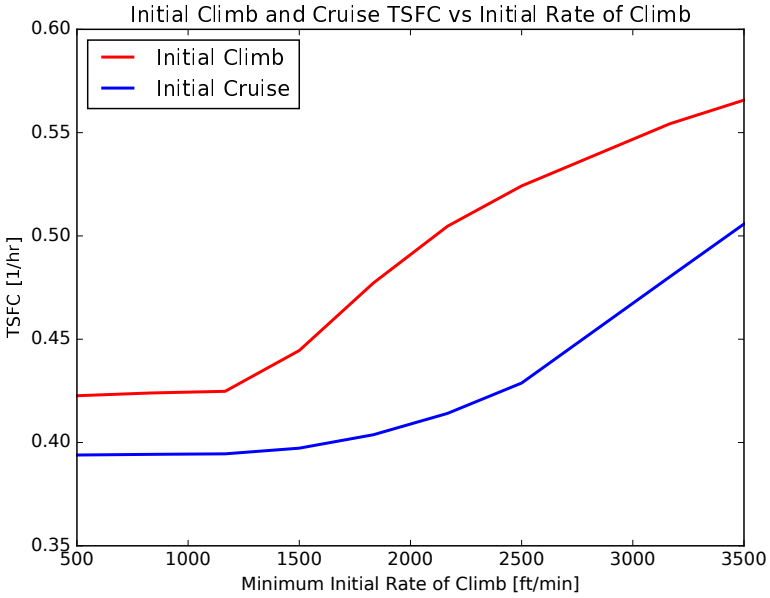

Fig. 14 Initial climb and cruise TSFC versus minimum initial climb rate.

Initially, it is quite beneficial to decrease the fan design pressure ratio, as indicated by the sensitivity of approximately 0.5. However, as the minimum climb rate increases and the max thrust requirement on the engine increases, it becomes less beneficial to decrease the fan design pressure ratio. This is indicated by the decrease in sensitivity to approximately 0.1.

VII. Conclusion

This paper has presented a full 1D core+fan flowpath physics based, signomial programming compatible, turbofan model that was successfully validated against TASOPT and two NASA NPSS

Table 16 Top engine design value sensitivities in the aircraft optimization example for a single 2,000 nm mission.

Symbol	Description	Sensitivity
f_o	1 Minus Percent Mass Flow Bled	-2.600
η_{HPshaft}	High Pressure Shaft Power Transmission Efficiency	-1.50
π_{D}	Diffuser Pressure Ratio	-1.40
η_{B}	Combustor Efficiency	-1.10
π_{fn}	Fan Duct Pressure Loss	-0.99
η_{LPshaft}	Low Pressure Shaft Power Transmission Efficiency	-0.86
π_{b}	Burner Pressure Ratio	-0.41
π_{f_D}	On Design Fan Pressure Ratio	0.50

Table 17 Top aircraft design and mission parameter sensitivities in the aircraft optimization example.

Variable	Description	Sensitivity
e	Oswald Efficiency Factor	-0.45
W_{pax}	Passenger Weight	0.65
Rng	Required Range	0.95

models. The model is meant to be combined with other aircraft subsystem models to perform full system optimization. Using GPKit's performance modeling framework, the turbofan model was formulated as a unified multi-point optimization problem with no on/off design point distinction or order of operations. The model can be easily be integrated into a full aircraft optimization model. This was demonstrated by integrating the turbofan model into a simple commercial aircraft sizing model and performing a series of parametric studies, including a 2,460 variable multi-mission optimization problem that solves in 28 seconds.

Appendix

Appendix Nomenclature

A_{fuse} = projected fuselage area
A_{pax} = required fuselage are per passenger
AR = wing aspect ratio
b = wing span
b_{max} = max allowed wing span
$C_{d_{\text{fuse}}}$ = fuselage drag coefficient
C_{d_w} = wing drag coefficient
D_i = total aircraft drag in segment i
ΔH_i = altitude change during segment i
N_{eng} = aircraft's number of engines
N_{pax} = aircraft's numer of passengers
θ_i = segment i climb angle
h_i = segment i altitude
P_{excess} = segment i excess power
Range_i = distance covered during segment i
RC_i = segment i rate of climb
S = wing planform area
t = segment i duration
V_{stall} = aircraft stall speed
W_{avg_i} = average segment aircraft weight
W_{end_i} = aircraft weight at end of segment i
W_{fuel_i} = fuselage weight burned during segment i
$W_{\text{fuel}_{\text{total}}}$ = total fuel weight
W_{fuse} = fuselage weight
W_{pax} = passenger weight

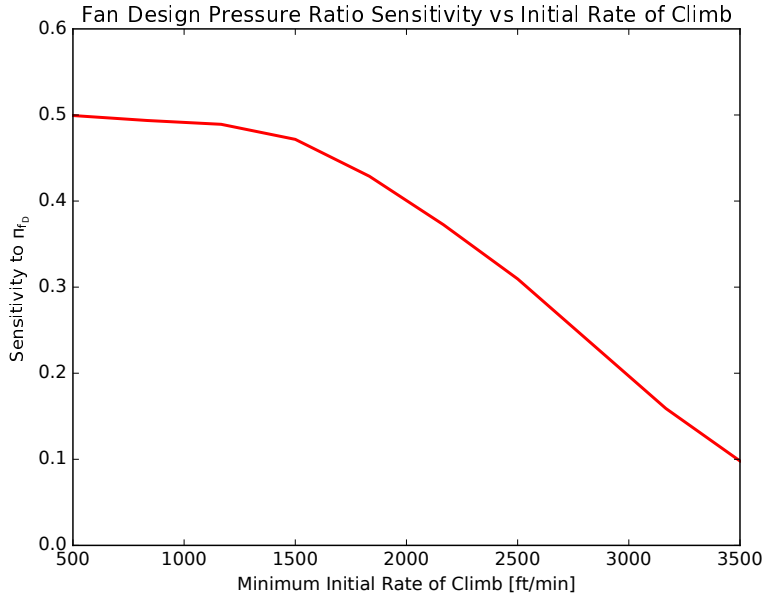

Fig. 15 Sensitivity to fan design pressure ratio versus minimum initial climb rate.

W_{payload} = payload weight
W_{S_i} = segment i wing loading
$W_{S_{\max}}$ = max allowed wing loading
W_{start_i} = aircraft weight at start of segment i
W_{TO} = takeoff weight
W_{wing} = wing weight
z_{bre} = Breguet parameter

A. Flight Profile and Aircraft Sizing Model

The aircraft sizing model and flight profile model sizes a commercial aircraft for minimum fuel burn during a flight of user specified range. The model is discretized into a user selected number of climb and cruise flight segments. Descent is neglected. To avoid introducing a signomial, the downrange distance traveled during climb does not contribute to total mission range.

1. Weight Breakdown

The payload is taken to be only passengers and their baggage. Per passenger total weight (person + baggage) is assumed to be 210 pounds and the number of passengers, N_{pax}, is specified by the user. The empty fuselage and tail weight is approximated as 75 percent of the payload weight. The 75 percent fraction is estimated from TASOPT 737 output. Wing weight is computed using a simplified Raymer wing weight equation normalized by TASOPT 737 wing weight, area, and aspect ratio values[20] in Equation 82. Total fuel burn is the sum of segment fuel burn.

$$W_{\text{payload}} = W_{\text{pax}} N_{\text{pax}} \tag{80}$$

$$W_{\text{fuse}} = 0.75 W_{\text{payload}} \tag{81}$$

$$\left(\frac{S}{124.58\text{m}^2}\right)^{0.65}\left(\frac{AR}{10.1}\right)^{0.5} = \frac{W_{\text{wing}}}{105384.1524\text{N}} \tag{82}$$

$$W_{\text{fuel}_i} = N_{\text{eng}}\text{TSFC}_i t_i F_i \tag{83}$$

$$W_{\text{fuel}_{\text{total}}} \geq \sum_{n=1}^{N} W_{\text{fuel}_i} \tag{84}$$

The aircraft's take off weight is the sum of all previously computed weights. Engine weight, W_{eng}, is set by the linked turbofan model. N_{eng} is the user input number of engines.

$$W_{\text{TO}} \geq W_{\text{fuse}} + W_{\text{payload}} + W_{\text{fuel}_{\text{total}}} + N_{\text{eng}}W_{\text{eng}} + W_{\text{wing}} \tag{85}$$

Equations 86 through 88 set each flight segment's start and end weight.

$$W_{\text{start}_i} = W_{\text{end}_{i-1}} \tag{86}$$

$$W_{\text{start}_0} = W_{\text{TO}} \tag{87}$$

$$W_{\text{end}_i} \geq W_{\text{empty}} + W_{\text{payload}} + N_{\text{eng}}W_{\text{eng}} + W_{\text{wing}} \tag{88}$$

In later constraints, W_{avg_i}, the geometric mean of a segments start and end weight, is used instead of either the segment start or end weight. This increases accuracy and is more sTable than using segment start or end weight.

$$W_{\text{avg}_i} = \sqrt{W_{\text{start}_i}W_{\text{end}_i}} \tag{89}$$

2. Aircraft Sizing

To capture landing/takeoff constraints wing loading is constrained to be less than a user specified max value. Aspect ratio, AR, is set by the wing span and wing area and constrained to be less than a user input maximum value. There is no wing structural model. Without the user input max value aspect ratio would grow unrealistically large.

$$W_{\text{S}_\text{i}} = \frac{\frac{1}{2}C_{L_i}S\rho_i(V_i)^2}{S} \tag{90}$$

$$W_{\text{S}_\text{i}} \leq W_{\text{S}_{\text{max}}} \tag{91}$$

$$AR = \frac{b^2}{S} \tag{92}$$

$$AR \leq AR_{\text{max}} \tag{93}$$

In order to capture trends in fuselage drag, the fuselage is approximated as a flat plate. The plate's area is a function of number of passengers; the area per passenger, N_{pax} is estimated as $1m^2$/passenger. The estimate is based off the per passenger projected fuselage areas of late model 737 and 777s.

$$A_{\text{fuse}} = A_{\text{pax}} N_{\text{pax}} \tag{94}$$

The drag coefficient of a turbulent flat plate parallel to the free stream is 0.005. Fuselage drag can then be approximated as $C_{d_{\text{fuse}}} = \frac{1}{2}\rho V^2 A_{\text{fuse}} C_{d_{\text{fuse}}}$ where $C_{d_{\text{fuse}}} = 0.005$.

3. General Aircraft Performance

A number of constraints apply to both the climb and cruise portions of the flight. The speed of sound, velocity, and Mach number are computed for each flight segment. Velocity is also constrained to be greater than a user input stall speed. Segment lift, $\frac{1}{2}\rho_i C_{L_i}(V_i)^2$, is equated to the segments average weight.

$$a_i = \sqrt{\gamma R T_i} \tag{95}$$

$$V \geq V_{\text{stall}} \tag{96}$$

$$V_i = a_i M_i \tag{97}$$

$$W_{\text{avg}_i} = \frac{1}{2}\rho_i C_{L_i}(V_i)^2 \tag{98}$$

Drag is computed with Equation 100. The parabolic drag model, with the induced drag parameter K, is used to model induced drag. GPfit[14, 15] was used to develop a GP compatible fit to Xfoil[21] drag data for an NC130 airfoil[4] at a Reynolds number of 20 million. The fit is plotted in Figure 16. Equation 99, which sets C_{d_w}, was derived from the data fit.

$$C_{d_w} \geq (1.025e10){C_L}^{15.58} M^{156.86} + (2.856e{-}13){C_L}^{1.28} M^{6.25} + (2.091e{-}14){C_L}^{0.88} M^{0.03} + (1.944e6){C_L}^{5.65} M^{146.52} \tag{99}$$

$$D_i \geq (\frac{1}{2}\rho_i (V_i)^2)(C_{d_w} + K(C_L)^2 + C_{D_{\text{fuse}}} A_{\text{fuse}}) \tag{100}$$

$$K = (\pi e AR)^{-1} \tag{101}$$

4. Climb

The climb rate is set with an excess power formulation[22] and constrained to be greater than 500 ft/min. Equation 105 uses a small angle approximation to set the climb angle, θ.

$$P_{\text{excess}} + V_i D_i \leq V_i N_{\text{eng}} F_i \tag{102}$$

$$\text{RC}_i = \frac{P_{\text{excess}}}{W_{\text{avg}_i}} \tag{103}$$

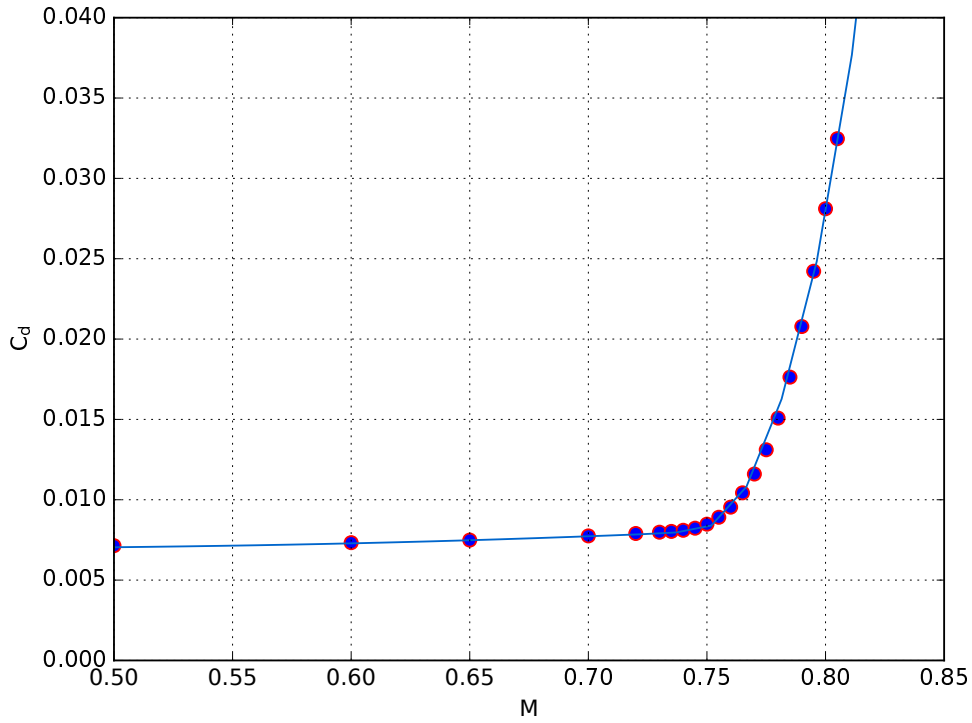

Fig. 16 Xfoil NC130 airfoil drag data (dots) and a posynomial approximation of the data (solid line) for a Reynolds number of 20 million.

$$\mathrm{RC}_i \geq 500 \quad \mathrm{ft/min} \tag{104}$$

$$\theta_i V_i = \mathrm{RC}_i \tag{105}$$

Altitude change during each climb segment is a function of climb rate and total segment time. Equation 107 uses a small angle approximation to compute the downrange distance covered during a climb segment. This distance is not credited towards the aircraft's mission range.

$$\Delta H_i = t_i \mathrm{RC}_i \tag{106}$$

$$t_i V_i = \mathrm{Range}_i \tag{107}$$

During climb there is a downward pressure on each segment's end altitude (climbing extra burns more fuel). This allows each climb segments end altitude to be computed with equation 108.

$$h_i \geq h_{i-1} + \Delta H_i \tag{108}$$

5. Cruise

During cruse, steady level flight conditions are assumed and segment duration is constrained via equation 110. This is the same equation as 107, except it does not use a small angle approximation.

$$D_i = N_{\text{eng}} F_i \tag{109}$$

$$t_i V_i = \text{Range}_\text{i} \tag{110}$$

The Breguet Range equation (Equation 111) is used to model cruise fuel burn. However, the natural logarithm in Equation 111 is not GP compatible and must be reformulated using the procedure outlined by Hoburg et al[2]. Equations 112 and 113 constitute the reformulated Breguet range equation. W_i in equation 111 has been replaced with W_{avg_i} to increase accuracy.

$$ln\left(\frac{W_{\text{start}_i}}{W_{\text{end}_i}}\right) = \frac{D_i(\text{TSFC}_i t_i)}{W} \tag{111}$$

$$z_{\text{bre}} + \frac{{z_{\text{bre}}}^2}{2} + \frac{{z_{\text{bre}}}^3}{6} \leq \frac{W_{\text{fuel}}}{W_{\text{end}}} \tag{112}$$

$$z_{\text{bre}} \geq \frac{D_i(\text{TSFC}_i)}{W_{\text{avg}_i}} t_i \tag{113}$$

6. Atmosphere Model

Equation 114, a signomial equality, is used to compute each flight segment's temperature (h is linked to segment end altitude). Atmospheric pressure is computed with the hydrostatic equation and density is computed with the ideal gas law. L_{atm} is the standard temperature lapse rate (0.0065 K/m), R is the univerals gas constant, M is the gasses molar mass, T_{SL} is sea-level temperature, and P_{SL} is the sea level pressure.

$$T_{\text{SL}} = T + L_{\text{atm}} h \tag{114}$$

$$\left(\frac{P}{P_{\text{SL}}}\right)^{\frac{LR}{g}} = \frac{T}{T_{\text{SL}}} \tag{115}$$

$$\rho = \frac{P}{(R/M)T} \tag{116}$$

B. Equality Constraint Intuition

Equality constraints are required when one variable is being pressured in multiple different directions. Consider the constraints used in a simple atmosphere model integrated into an aircraft mission profile. L is the standard the temperature lapse rate of 0.0065 K/m and T_{SL} and P_{SL} are the sea level temperature and pressure, respectively.

$$\rho = \frac{P}{RT}, \qquad \left(\frac{P}{P_{\text{SL}}}\right)^{\frac{LR}{g}} = \frac{T}{T_{\text{SL}}}, \qquad T_{\text{SL}} = T + Lh \tag{117}$$

It is not clear apriori how to relax the posynomial equality $T_{\text{SL}} = T + Lh$ to an inequality. During the climb phase of the flight, there will be an upwards pressure on density (higher density allows a higher climb rate) creating a downwards pressure on T. During the cruise portion of the flight, there will be a downward pressure on density (lower density produces less drag on the aircraft) creating an upwards pressure on T. Situations like this require signomial equality constraints.

Acknowledgments

This work was partially funded by Aurora Flight Sciences.

References

[1] Martins, J. R. and Lambe, A. B., "Multidisciplinary Design Optimization: A survey of Architectures," *AIAA Journal*.

[2] Hoburg, W. and Abbeel, P., "Geometric Programming for Aircraft Design Optimization," *AIAA Journal*.

[3] Kirschen, P. G., Burnell, E. E., and Hoburg, W. W., "Signomial Programming Models for Aircraft Design," *AIAA SciTech*.

[4] Drela, M., "N3 Aircraft Concept Designs and Trade Studies - Appendix. Technical Report NASA CR-2010-216794/VOL2," Tech. rep., NASA, 2010.

[5] Institute, S. R., "Numerical Propulsion System Simulation," `http://www.swri.org/npss/purchase.asp`.

[6] Burnell, E. and Hoburg, W., "GPkit software for geometric programming," `https://github.com/hoburg/gpkit`, 2015. Version 0.4.0.

[7] ApS, "The MOSEK C optimizer API manual," , 2015. Version 7.1 (Revision 41).

[8] Duffin, R., Peterson, E., and Zener, C., *Geometric programming: theory and application,*, Wiley New York, 1967.

[9] Boyd, S. and Vandenberghe, L., *Convex Optimization*, Cambridge University Press, The address, 7th ed., 2009.

[10] Boyd, S., Kim, S.-J., Vanderberghe, L., and Hassibi, A., "A tutorial on geometric programming," *Optim Eng*.

[11] Lipp, T. and Boyd, S., "Variations and extension of the convex concave procedure," *Optim Eng*.

[12] Opgenoord, M. M., Cohen, B. S., and Hoburg, W. W., "Equality Constraints for Signomial Programming," *Optim Eng*.

[13] GeneralElectric, "Energy Efficient Engine Flight Propulsion System Aircraft/Engine Integration Evaluation," Tech. rep., NASA, 1980.

[14] Hoburg, W., Kirschen, P., and Abbeel, P., "Data fitting with geometric-programming-compatible softmax functions," *Optim Eng*.

[15] Kirschen, P. and Hoburg, W., "GPfit," `https://github.com/convexopt/gpfit`, 2015. Version 0.1.

[16] Marvis, D., "Environmental Design Space (EDS) Overview," Tech. rep., Presentation to the Transportation Research Board, Papers and Briefings on the Development Program for the Aviation Environmental Tool Suite, Workshop no. 4, Dec. 6-8, 2006, URL: `http://www.faa.gov/about/office_org/headquarters_offices/apl/research/models/history/media/05_DM_Overview-EDS_2006-11-28_FINAL.pdf`, 2010.

[17] `https://www.cfmaeroengines.com/engines/cfm56/`.

[18] Mobil, E., "Jet Fuel Product Properties," `https://www.exxonmobil.com/English-FI/Commercial-Fuel/pds/GLXXJetFuel-Series`.

[19] Yutko, B., *The Impact of Aircraft Design Reference Mission on Fuel Efficiency in the Air Transportation System*, Ph.D. thesis, Massachussets Institute of Technology, 2013.

[20] Raymer, D. P., *Aircraft Design: A Conceptual Approach*, American Institute of Aeronautics and Astronautics, Reston, Virginia, 4th ed., 2006.

[21] Drela, M., "XFOIL: An Analysis and Design System for Low Reynolds Number Airfoils," in "Low Reynolds Number Aerodynamics," Springer, pp. 1–12, 1989.

[22] Anderson, J. D., *Aircraft Performance and Design*, WCB McGraw-Hill, Boston, Massachusetts, 1999.